Hindawi Publishing Corporation
Journal of Nanotechnology
Volume 2012, Article ID 214783, 7 pages
doi:10.1155/2012/214783

Research Article

Fabrication of Bi-Doped TiO_2 Spheres with Ultrasonic Spray Pyrolysis and Investigation of Their Visible-Light Photocatalytic Properties

Jianhui Huang,[1,2] Wahkit Cheuk,[2] Yifan Wu,[3] Frank S. C. Lee,[3] and Wingkei Ho[2,3]

[1] *Department of Environmental and Life Sciences, Putian University, Putian 351100, China*
[2] *Nano and Advanced Materials Institute Limited, The Hong Kong University of Science and Technology, Hong Kong*
[3] *Department of Civil and Structural Engineering, Research Center for Environmental Technology and Management, The Hong Kong Polytechnic University, Hong Kong*

Correspondence should be addressed to Jianhui Huang, owenhuang95@163.com and Wingkei Ho, howingkei@gmail.com

Received 8 March 2012; Accepted 20 April 2012

Academic Editor: Reda M. Mohamed

Bismuth-doped TiO_2 submicrospheres were synthesized by ultrasonic spray pyrolysis. The prepared bismuth-doped titania was characterized by X-ray diffraction (XRD), scanning electron microscopy (SEM), transmission electron microscopy (TEM), UV-visible diffuse reflectance spectroscopy (UV-vis DRS), and X-ray photoelectron spectroscopy (XPS). Aqueous photocatalytic activity was evaluated by the decomposition of methyl orange under visible-light irradiation. The results indicate that doping of bismuth remarkably affects the phase composition, crystal structure, and the photocatalytic activity. The sample with 2% Bi exhibits the optimum photocatalytic activity.

1. Introduction

Photocatalytic oxidation of pollutants has increasing interests in recent years because of its advantages such as high redox capability, nonselectivity, and efficient solar utilization. Different kinds of photocatalytic materials have been studied such as metal oxides, nitrides, and sulfides [1–7]. Among them, TiO_2 is the most commonly used photocatalyst owing to its high redox power, photostability, chemical inertness and low cost. However, the relatively low quantum efficiency of TiO_2 photocatalysts limits its real application. To overcome this problem, a lot of efforts have been paid to improve the photocatalytic efficiency of TiO_2 from the viewpoint of practical use.

It has been reported that the crystal size, specific surface area, morphology, and texture have great effects on the photocatalytic properties of semiconductors. Nano/microspheres structure has attracted great interests due to their thermodynamically favorable state in terms of surface energy. Recent researches have demonstrated their potential application in many fields such as photonic crystals [8], biomedicine [9, 10], sensing [11, 12], and solar cells [13, 14]. In particular, some studies found that the nano/microspheres structure of semiconductor have promising properties in the region of photocatalysis [15–17]. Various approaches have been used for the preparation of spherical semiconductor materials. The most common approach is based on the use of various removable templates. The removal of template materials is complex and usually requires high temperature processes or wet chemical etching, which is expensive and not easy for mass application. Therefore, it is promising to develop a simple and inexpensive way without using template for the preparation of semiconductor nano/microspheres.

Many reports have shown that the photocatalytic properties of TiO_2 can be modified strongly by doping with different elements. The doping element at low concentrations can act as separation centers for the light-induced electron-hole pairs, prohibiting the undesirable fast recombination of the electron-hole pairs. Besides, the doping of impurity atoms has also been proven for the extension of the optical absorption of photocatalysts [18–20]. Thus, visible light in

the solar energy could be utilized. Among various transition metals, bismuth is a good choice as the dopants in photocatalysis research. Many bismuth-based semiconductors such as Bi_2O_3 [21], BiOCl [22], $BiVO_4$ [23–25], Bi_2WO_6 [26], and Bi_2MoO_6 [27] have been found to be efficient as visible-light-driven photocatalysts. Research studies also reported that bismuth-doped materials have enhanced photocatalytic activity [28–31]. For example, Li and his coworkers prepared Bi-doped TiO_2 exhibiting high efficiency in the decomposition of benzene under the irradiation of visible-light [32]. Liu et al. reported that Bi_2O_3-TiO_2 composite also showed high visible light photocatalytic activity in the degradation of methyl orange [33].

In this study, we described the synthesis of Bi-doped TiO_2 spheres with a doping level in the range of 0.5–5% via a facile method of ultrasonic spray pyrolysis. Their photocatalytic performance in the decomposition of methyl orange (MO) dye under visible light irradiation was also investigated.

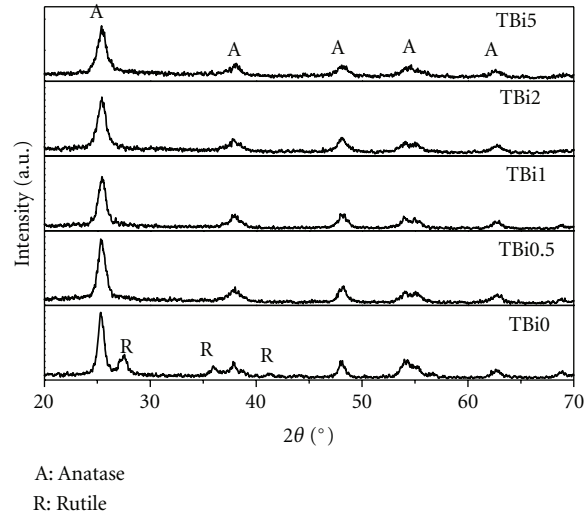

Figure 1: XRD patterns of Bi-doped TiO_2 spheres with 0, 0.5, 1, 2, and 5% of Bi.

2. Experimental Section

2.1. Catalysts Preparation. All the chemicals were of commercially available analytical grade and used without further purification. Bi-doped TiO_2 photocatalysts were prepared by an ultrasonic spray pyrolysis method. In a typical process, 2.2 mL $TiCl_4$ was added to 200 mL HCl solution (0.5 M) under magnetic stirring. After stirring for 1 hour, a transparent colorless solution was formed. The calculated amounts of Bismuth nitrate ($Bi(NO_3)_3 \cdot 6H_2O$) were added to the solution under magnetic stirring. After the Bismuth nitrate dissolved completely, the resulting solution was nebulized at 1.7 MHz ± 10%. The produced aerosol was carried through a corundum tube surrounded by a thermostated furnace with pumping air flow of 10 L/min. The pyrolysis proceeded quickly as aerosol passed through the high-temperature tube maintained at the temperatures of 500°C. The products were collected with distilled water and then separated by centrifugation. Collected samples were washed with water and ethanol and then dried at 80°C. The as-prepared product was then further calcined at 500°C and held for 2 h with a ramp rate of 3°C/min. The samples prepared with the doping level of 0, 0.5, 1, 2 and 5% were designated as TBi0, TBi0.5, TBi1, TBi2, and TBi5, respectively.

2.2. Characterization. X-ray diffraction (XRD) patterns were collected using a Bruker D8 Advance X-ray diffractometer (Cu $K_{\alpha 1}$ irradiation, λ = 1.5406 Å). SEM images of the samples were performed on a JEOL JSM-6300 microscope operated at an accelerating voltage of 15 kV. Transmission electron microscopic (TEM) images were obtained on JEOL 2010F TEM microscope operated at an accelerating voltage of 200 kV. A Varian Cary 500 Scan UV/vis system equipped with a Labsphere diffuse reflectance accessory was used to obtain the reflectance spectra of the catalysts. XPS experiments were performed on a Physical Electronics PHI 5600 multitechnique system, using monochromatized Al K_α radiation (1486.6 eV) at 350 W.

2.3. Evaluation of Photocatalytic Activity. The photocatalytic activities of the samples were evaluated by the decomposition of methyl orange (MO) in aqueous solution. Catalyst (0.04 g) was suspended in a 100 mL Pyrex glass vessel containing contaminant aqueous solution. The initial concentration of MO is 10 ppm. The visible-light source was a 300 W halogen lamp (Philips Electronics) positioned beside a cylindrical reaction vessel with a flat side. The system was water-cooled to maintain the temperature. A 400 nm cutoff filter was placed in front of the vessel to ensure irradiation by visible light. The suspension was stirred in darkness for 2 h to achieve adsorption equilibrium, and the reactor was irradiated to induce photocatalyzed decomposition reactions. At given irradiation time intervals, 3 mL of the reaction suspension was collected and centrifuged to remove the catalyst. The degraded solution was analyzed using a Varian Cary 50 Scan UV/vis spectrophotometer.

3. Results and Discussion

3.1. Crystal Structure and Morphology. Figure 1 shows the X-ray diffraction (XRD) patterns of the samples doped with different amounts of Bi. It indicates that the amount of Bi plays an important role in controlling the crystal structure of the products. For the undoped sample, both anatase and rutile are found while the doped samples only exist in anatase phase. The peak intensity of anatase becomes weaker with increasing the content of Bi dopant, while the width of the (101) peak becomes broader. The calculated average crystal sizes of the TBi0, TBi0.5, TBi1, TBi2, and TBi5 using the Scherrer equation are 12.7, 10.4, 9.8, 9.3, and 8.6 nm, respectively, indicating the nanocrystal nature of the prepared samples. The result also indicates that the doping of Bi could suppress the agglomeration of TiO_2 particle during the thermal treatment and enhance the phase transformation temperature.

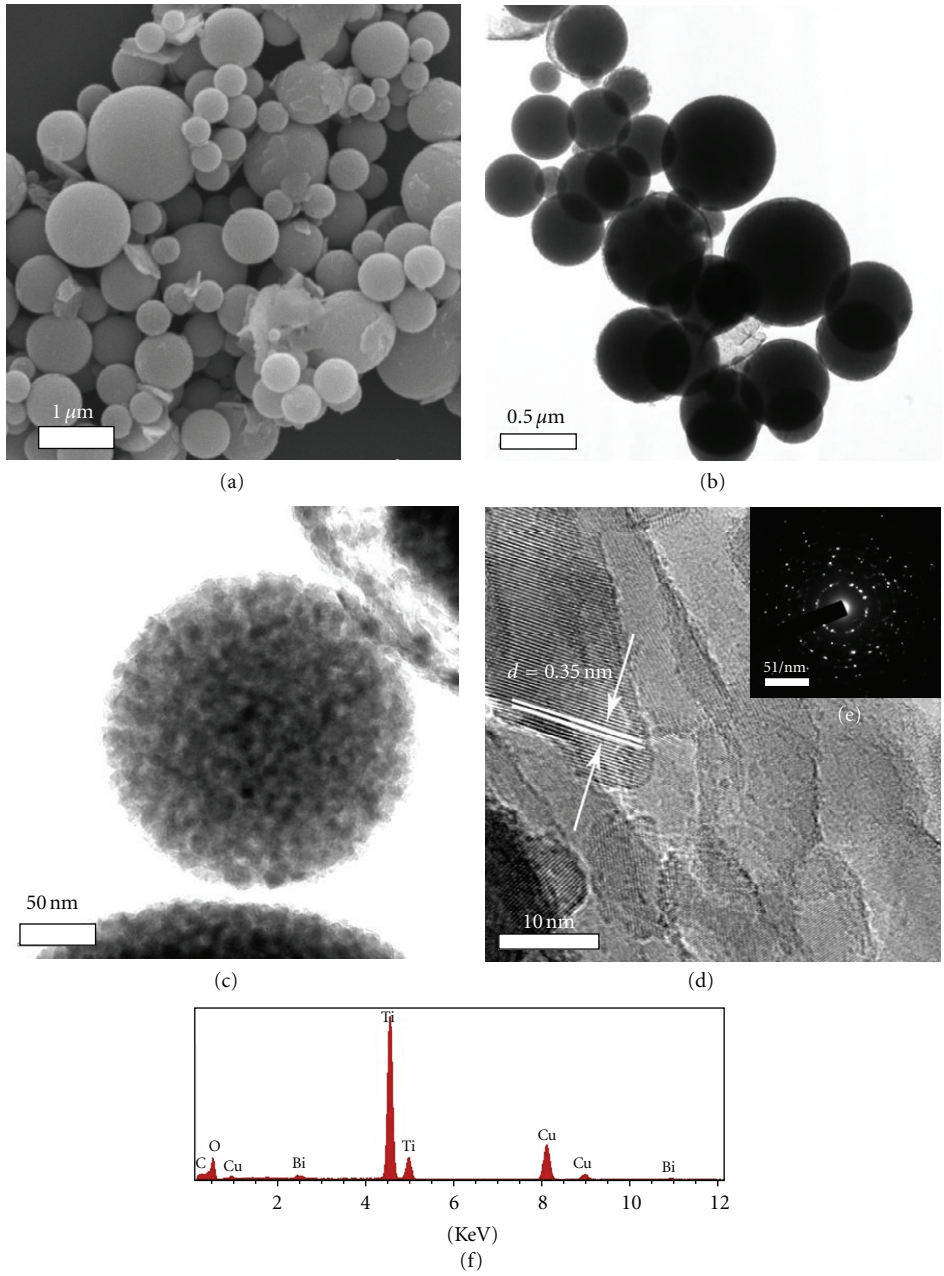

Figure 2: Representative structural characterizations and general morphologies of Bi-doped TiO_2 with 2% of Bi (a) SEM image, (b) and (c) TEM images, (d) HRTEM image, (e) SAED pattern, and (f) Energy-dispersive X-ray analysis spectra.

Figures 2(a) and 2(b) depict the SEM and TEM images of doped TiO_2 with 2% Bi, respectively. The images show that the as-prepared samples consist entirely of spheres with a range of 100 nm to 1.5 μm. The ultrasonic nebulizer during the preparation is the key to form the spherical morphology. It is known that the droplets produced from nebulizer could serve as microreactors and yield the particle from each droplet when sprayed into a tubular reactor under pyrolysis conditions. In addition, the size of droplet determines the product dimension [34]. In Figure 2(c), the typical high magnified TEM image of Bi-doped TiO_2 spheres is shown, which reveals that the prepared spheres are composed of small nanoparticles and have porous structure. Figure 2(d) shows the HRTEM image at the edge of the Bi-doped TiO_2 spheres. Well-resolved lattice fringes are clearly observed, with an interplanar distance of 0.35 nm corresponding to the (101) d-spacing of the anatase phase. The selected area electron diffraction (SAED) pattern (Figure 2(e)) of the spheres demonstrates well crystalline nature of the doped TiO_2 spheres, which is in well agreement with the XRD results. The composition of the doped TiO_2 spheres was determined by energy dispersive X-ray spectroscopy (EDX). The results of EDX analysis (Figure 2(f)) imply that the as-prepared samples contain Ti, O, and a small amount of Bi

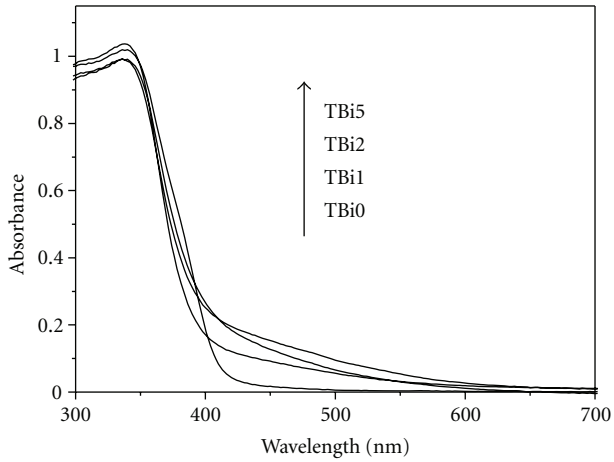

Figure 3: Diffuse reflectance UV-vis spectra of Bi-doped spherical TiO_2 and pure TiO_2.

element. The ratio of Bi to Ti in the produced nanocrystalline titania microspheres is 0.019, which is very close to that in the precursor solution. Therefore, the Bi concentration in the precursor solution could approximately represent the corresponding Bi concentration in the nanocrystalline titania spheres.

3.2. Optical Properties. Figure 3 shows the UV spectra of the doped samples with different amounts of Bi. Compared with the undoped sample, the Bi-doped TiO_2 samples show remarkable absorption in the visible-light region. The absorption in visible-light region is increased with the Bi-doping content. This wide visible-light response of Bi-doped TiO_2 spheres could attribute to the formation of surface-defect centers, which are associated with existence of oxygen vacancies created by the doping process [35, 36]. Besides, the basic adsorption edge of the Bi-doped TiO_2 is shifted to a shorter wavelength. These blue shifts of adsorption edge are possibly due to the quantum confinement effect, which is attributed to the smaller crystal size of Bi-doped samples.

3.3. Surface Electronic States and Composition. The assessment of the surface chemical composition and electronic state of the product was studied by XPS analysis. Figure 4(a) is the XPS survey spectrum of TBi2, which contains the peaks of Ti, O, Bi, and C elements. The C element can be ascribed to the adventitious hydrocarbon from the XPS instrument itself. The high-resolution XPS spectra of the Ti 2p, Bi 4f, and O 1s region on the surface of samples are shown in Figure 4(b)–4(d). In Figure 4(b), the two peaks at 459.0 and 464.8 eV are assigned to the Ti $2p_{3/2}$ and Ti $2p_{1/2}$ states in TiO_2, respectively. The binding energy of Ti 2p shows a positive shift of approximately 0.4 eV compared to those of pure anatase TiO_2, [37] implying the successful incorporation of the bismuth atom into the TiO_2 lattice. In Figure 4(c), four peaks could be found. The peaks centered at 164.9, 163.1, and 159.6, 157.9 eV could be assigned to Bi $4f_{5/2}$ and Bi $4f_{7/2}$, respectively, indicating two different states of Bi in the sample. The peaks of 163.1 and 157.9 eV could be attributed to the Bi^{3+}, which is in good agreement with other studies [38]. The peaks at high binding energy of 164.9 and 159.6 eV could be assigned to the Bi doped into the TiO_2 lattice. The doped Bi with a strong interaction between TiO_2 is oxidized to Bi^{4+} [39–41]. The presence of Bi^{4+}/Bi^{3+} species in the catalyst favors the trap of electrons and benefits the separation of the electron-hole pairs in the photocatalytic process. The O1s XPS spectra in the Figure 4(d) are asymmetric, which can be fitted by two peaks. The strong peak at the low binding energy of 530.0 eV corresponds to crystal lattice oxygen (Ti–O). The shoulder peak at 531.6 eV is associated with hydroxyl groups (H–O) [42, 43]. The quantitative XPS analysis shows that the surface atomic number ratio of Bi to Ti is close to 1.9 : 100, which is also near the ratio in the precursor. Both XPS and EDX results indicate that Bi is uniformly dispersed into the TiO_2.

3.4. Photocatalytic Activity. The photocatalytic performances of the doped photocatalysts were evaluated by comparing the degradation efficiency of methyl orange (MO) with otherwise identical conditions under visible-light irradiation ($\lambda >$ 400 nm) after the adsorption-desorption equilibrium was reached. Figure 5 shows the MO degradation C_t/C_0 (C_0 and C_t are the equilibrium concentration of MO before and after visible-light irradiation, resp.) versus visible-light irradiation time in the presence of various photocatalysts. Control test (without catalyst) under visible-light irradiation showed that the photolysis of MO was negligible. As expected, the doping of Bi greatly affects the photocatalytic activity of TiO_2 spheres. Only limited (~6%) MO was degraded over undoped TiO_2 spheres. For the doped samples, they show much higher decomposition rate. For the optimal catalyst (TBi2), over 90% MO was degraded after the irradiation of 12 h. The visible-light activity of doped TiO_2 may be attributed to two reasons. The first one is due to the formation of oxygen vacancy after introducing of bismuth leading to the visible-light response of TiO_2. Another reason is the introduction of Bi existed in two states of Bi^{4+} and Bi^{3+} as shown in the result of XPS. The Bi^{4+}/Bi^{3+} species trap the electrons and thus can be benefited from the separation of the electron-hole pairs.

The test also shows that the activities of doped samples were greatly influenced by the level of doped Bi. For the sample of TBi0.5, the decomposition of MO after 12 h reaction is as high as 40%. When the concentration of Bi in the doped TiO_2 is increased to 2%, the degraded MO is increased to 90%. Further increasing the level of Bi in the TiO_2 spheres, the efficiency drops quickly. When the dopant concentration increases to 5%, only 50% MO was degraded after 12 h photocatalytic reaction. It has been reported that the doping of transition metal serving as electron/hole separation centers can eliminate the rapid recombination of excited electron/hole pair during photoreaction, thereby increasing the efficiency of the TiO_2 photocatalyst. However, this effect is sensitive to dopant levels. The excessive dopants can act as recombination centers, promoting the recombination of electron/hole pairs. The activity of Bi-doped TiO_2

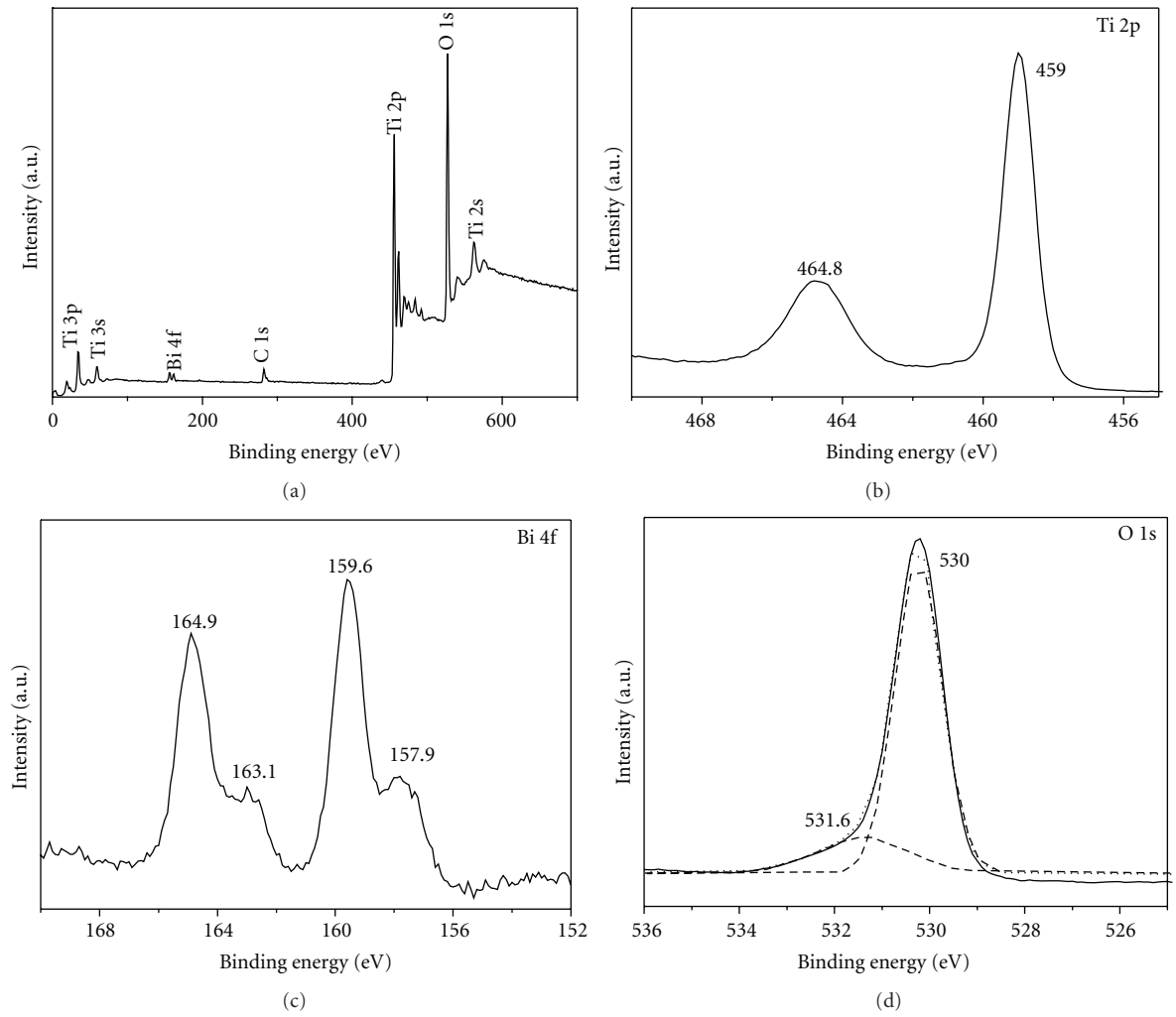

Figure 4: (a) XPS survey spectrum of TBi2, (b) high-resolution XPS spectrum of Ti 2p region, (c) high-resolution XPS spectrum of Bi 4f region, and (d) high-resolution XPS spectrum of O1s region of TBi2.

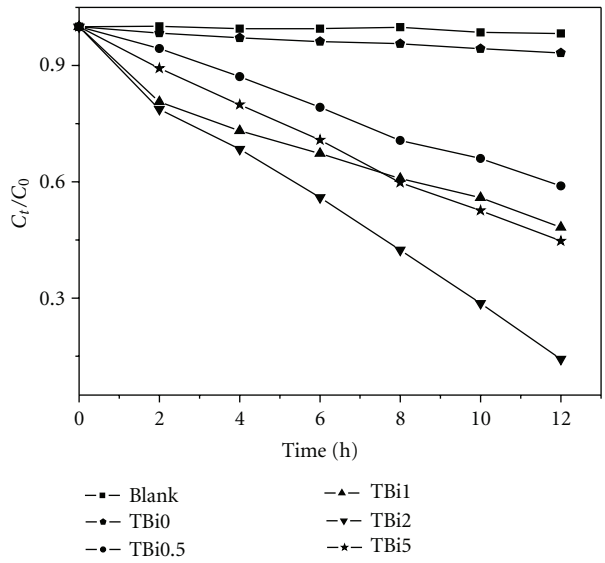

Figure 5: Photocatalytic activity of the Bi-doped TiO_2 spheres samples.

indicates that 2% is the optimized level, which may slow down the recombination process.

4. Conclusions

The Bi-doped TiO_2 spheres with variable Bi dopant concentrations were synthesized by using ultrasonic spray pyrolysis process. The doping of Bi effectively suppressed the formation of rutile phase and the crystal growth of TiO_2 particles during preparation. Bi-doped TiO_2 samples showed an extension of light absorption into the visible-light region. It exhibited improved photocatalytic activities in the degradation of methyl orange under visible-light irradiation. Compared with the traditional preparation technique of spherical materials, the ultrasonic spray pyrolysis technique presented in this paper is continuous and easily to be operated. We believe that this facile method is easy to scale up for industrial production. Similar doping or codoping with other nonmetal and metal ions with similar method would lead to the development of a new kind of materials.

Acknowledgments

The author would like to thank the support of the National Natural Science Foundation of China (21103095) and the Natural Science Foundation of Fujian Province (Grant no. 2010J05030).

References

[1] C. Shifu, C. Lei, G. Shen, and C. Gengyu, "The preparation of coupled WO_3/TiO_2 photocatalyst by ball milling," *Powder Technology*, vol. 160, no. 3, pp. 198–202, 2005.

[2] J. Zhang, X. Chen, K. Takanabe et al., "Synthesis of a carbon nitride structure for visible-light catalysis by copolymerization," *Angewandte Chemie*, vol. 49, no. 2, pp. 441–444, 2010.

[3] J. Zhang, J. Sun, K. Maeda et al., "Sulfur-mediated synthesis of carbon nitride: band-gap engineering and improved functions for photocatalysis," *Energy and Environmental Science*, vol. 4, no. 3, pp. 675–678, 2011.

[4] X. Chen, J. Zhang, X. Fu, M. Antonietti, and X. Wang, "Fe-g-C_3N_4-catalyzed oxidation of benzene to phenol using hydrogen peroxide and visible light," *Journal of the American Chemical Society*, vol. 131, no. 33, pp. 11658–11659, 2009.

[5] S. L. Wang, X. Jia, P. Jiang, H. Fang, and W. H. Tang, "Large-scale preparation of chestnut-like ZnO and Zn-ZnO hollow nanostructures by chemical vapor deposition," *Journal of Alloys and Compounds*, vol. 502, no. 1, pp. 118–122, 2010.

[6] X. Wang, K. Maeda, A. Thomas et al., "A metal-free polymeric photocatalyst for hydrogen production from water under visible light," *Nature Materials*, vol. 8, no. 1, pp. 76–80, 2009.

[7] J. Huang, Y. Cui, and X. Wang, "Visible light-sensitive ZnGe oxynitride catalysts for the decomposition of organic pollutants in water," *Environmental Science and Technology*, vol. 44, no. 9, pp. 3500–3504, 2010.

[8] Y. Wang, M. Ibisate, Z.-Y. Li, and Y. Xia, "Metallodielectric photonic crystals assembled from monodisperse spherical colloids of bismuth and lead," *Advanced Materials*, vol. 18, no. 4, pp. 471–476, 2006.

[9] W. Zhao, H. Chen, Y. Li, A. Li, M. Lang, and J. Shi, "Uniform rattle-type hollow magnetic mesoporous spheres as drug delivery carriers and their sustained-release property," *Advanced Functional Materials*, vol. 18, no. 18, pp. 2780–2788, 2008.

[10] J. E. Lee, N. Lee, H. Kim et al., "Uniform mesoporous dye-doped silica nanoparticles decorated with multiple magnetite nanocrystals for simultaneous enhanced magnetic resonance imaging, fluorescence imaging, and drug delivery," *Journal of the American Chemical Society*, vol. 132, no. 2, pp. 552–557, 2010.

[11] C. C. Li, X. M. Yin, T. H. Wang, and H. C. Zeng, "Morphogenesis of highly uniform $COCO_3$ submicrometer crystals and their conversion to mesoporous CO_3O_4 for gas-sensing applications," *Chemistry of Materials*, vol. 21, no. 20, pp. 4984–4992, 2009.

[12] J. Zhang, J. Liu, Q. Peng, X. Wang, and Y. Li, "Nearly monodisperse Cu_2O and CuO nanospheres: preparation and applications for sensitive gas sensors," *Chemistry of Materials*, vol. 18, no. 4, pp. 867–871, 2006.

[13] Q. Zhang, C. S. Dandeneau, S. Candelaria et al., "Effects of lithium ions on dye-sensitized ZnO aggregate solar cells," *Chemistry of Materials*, vol. 22, no. 8, pp. 2427–2433, 2010.

[14] Y. Kondo, H. Yoshikawa, K. Awaga et al., "Preparation, photocatalytic activities, and dye-sensitized solar-cell performance of submicron-scale TiO_2 hollow spheres," *Langmuir*, vol. 24, no. 2, pp. 547–550, 2008.

[15] G. Li, F. Liu, and Z. Zhang, "Enhanced photocatalytic activity of silica-embedded TiO_2 hollow microspheres prepared by one-pot approach," *Journal of Alloys and Compounds*, vol. 493, no. 1-2, pp. L1–L7, 2010.

[16] Y. Li, T. Sasaki, Y. Shimizu, and N. Koshizaki, "Hexagonal-close-packed, hierarchical amorphous TiO_2 nanocolumn arrays: transferability, enhanced photocatalytic activity, and superamphiphilicity without UV irradiation," *Journal of the American Chemical Society*, vol. 130, no. 44, pp. 14755–14762, 2008.

[17] C. Guo, M. Ge, L. Liu, G. Gao, Y. Feng, and Y. Wang, "Directed synthesis of mesoporous TiO_2 microspheres: catalysts and their photocatalysis for bisphenol A degradation," *Environmental Science and Technology*, vol. 44, no. 1, pp. 419–425, 2010.

[18] M. C. Wang, H. J. Lin, and T. S. Yang, "Characteristics and optical properties of iron ion (Fe^{3+})-doped titanium oxide thin films prepared by a sol-gel spin coating," *Journal of Alloys and Compounds*, vol. 473, no. 1-2, pp. 394–400, 2009.

[19] T. Kamegawa, J. Sonoda, K. Sugimura, K. Mori, and H. Yamashita, "Degradation of isobutanol diluted in water over visible light sensitive vanadium doped TiO_2 photocatalyst," *Journal of Alloys and Compounds*, vol. 486, no. 1-2, pp. 685–688, 2009.

[20] C. M. Teh and A. R. Mohamed, "Roles of titanium dioxide and ion-doped titanium dioxide on photocatalytic degradation of organic pollutants (phenolic compounds and dyes) in aqueous solutions: a review," *Journal of Alloys and Compounds*, vol. 509, no. 5, pp. 1648–1660, 2011.

[21] Z. Ai, Y. Huang, S. Lee, and L. Zhang, "Monoclinic α-Bi_2O_3 photocatalyst for efficient removal of gaseous NO and HCHO under visible light irradiation," *Journal of Alloys and Compounds*, vol. 509, no. 5, pp. 2044–2049, 2011.

[22] F. Chen, H. Liu, S. Bagwasi, X. Shen, and J. Zhang, "Photocatalytic study of BiOCl for degradation of organic pollutants under UV irradiation," *Journal of Photochemistry and Photobiology A*, vol. 215, no. 1, pp. 76–80, 2010.

[23] A. Kudo, K. Omori, and H. Kato, "A novel aqueous process for preparation of crystal form-controlled and highly crystalline

$BiVO_4$ powder from layered vanadates at room temperature and its photocatalytic and photophysical properties," *Journal of the American Chemical Society*, vol. 121, no. 49, pp. 11459–11467, 1999.

[24] L. Li and B. Yan, "$BiVO_4/Bi_2O_3$ submicrometer sphere composite: microstructure and photocatalytic activity under visible-light irradiation," *Journal of Alloys and Compounds*, vol. 476, no. 1-2, pp. 624–628, 2009.

[25] C.-Y. Chung and C.-H. Lu, "Reverse-microemulsion preparation of visible-light-driven nano-sized $BiVO_4$," *Journal of Alloys and Compounds*, vol. 502, no. 1, pp. L1–L5, 2010.

[26] L. Wu, J. Bi, Z. Li, X. Wang, and X. Fu, "Rapid preparation of Bi_2WO_6 photocatalyst with nanosheet morphology via microwave-assisted solvothermal synthesis," *Catalysis Today*, vol. 131, no. 1–4, pp. 15–20, 2008.

[27] L. Wu, J. Bi, J. Li, Z. Li, X. Wang, and X. Fu, "Simple solvothermal routes to synthesize nanocrystalline Bi_2MoO_6 photocatalysts with different morphologies," *Acta Materialia*, vol. 55, no. 14, pp. 4699–4705, 2007.

[28] Q. Yang, C. Xie, Z. Xu, Z. Gao, and Y. Du, "Synthesis of highly active sulfate-promoted Rutile Titania nanoparticles with a response to visible light," *Journal of Physical Chemistry B*, vol. 109, no. 12, pp. 5554–5560, 2005.

[29] J. Yu, S. Liu, Z. Xiu, W. Yu, and G. Feng, "Combustion synthesis and photocatalytic activities of Bi^{3+}-doped TiO_2 nanocrystals," *Journal of Alloys and Compounds*, vol. 461, no. 1-2, pp. L17–L19, 2008.

[30] S. Rengaraj and X. Z. Li, "Enhanced photocatalytic reduction reaction over Bi^{3+}-TiO_2 nanoparticles in presence of formic acid as a hole scavenger," *Chemosphere*, vol. 66, no. 5, pp. 930–938, 2007.

[31] W.-J. Hong and M. Kang, "The super-hydrophilicities of Bi-TiO_2, V-TiO_2, and Bi-V-TiO_2 nano-sized particles and their benzene photodecompositions with H_2O addition," *Materials Letters*, vol. 60, no. 9-10, pp. 1296–1305, 2006.

[32] H. Li, D. Wang, P. Wang, H. Fan, and T. Xie, "Synthesis and studies of the visible-light photocatalytic properties of near-monodisperse Bi-doped TiO_2 nanospheres," *Chemistry*, vol. 15, no. 45, pp. 12521–12527, 2009.

[33] Y. Liu, F. Xin, F. Wang, S. Luo, and X. Yin, "Synthesis, characterization, and activities of visible light-driven Bi_2O_3-TiO_2 composite photocatalysts," *Journal of Alloys and Compounds*, vol. 498, no. 2, pp. 179–184, 2010.

[34] J. Zhang, A. Elsanousi, J. Lin et al., "Aerosol-assisted self-assembly of aluminum borate ($Al_{18}B_4O_{33}$) nanowires into three dimensional hollow spherical architectures," *Crystal Growth and Design*, vol. 7, no. 12, pp. 2764–2767, 2007.

[35] S. M. Prokes, J. L. Gole, X. Chen, C. Burda, and W. E. Carlos, "Defect-related optical behavior in surface-modified TiO_2 nanostructures," *Advanced Functional Materials*, vol. 15, no. 1, pp. 161–167, 2005.

[36] V. N. Kuznetsov and N. Serpone, "Visible light absorption by various titanium dioxide specimens," *Journal of Physical Chemistry B*, vol. 110, no. 50, pp. 25203–25209, 2006.

[37] J. F. Moulder, W. F. Stickle, P. E. Sobol, and K. D. Bomben, in *Handbook of X-ray Photoelectron Spectroscopy*, J. Chastain, Ed., Perkin-ElmerCorporation, Eden Prairie, Minn, USA, 1992.

[38] K. Brezesinski, R. Ostermann, P. Hartmann, J. Perlich, and T. Brezesinski, "Exceptional photocatalytic activity of ordered mesoporous β-Bi_2O_3 thin films and electrospun nanofiber mats," *Chemistry of Materials*, vol. 22, no. 10, pp. 3079–3085, 2010.

[39] H. Li, D. Wang, P. Wang, H. Fan, and T. Xie, "Synthesis and studies of the visible-light photocatalytic properties of near-monodisperse Bi-doped TiO_2 nanospheres," *Chemistry*, vol. 15, no. 45, pp. 12521–12527, 2009.

[40] Y. Wang, Y. Wang, Y. Meng et al., "A highly efficient visible-light-activated photocatalyst based on bismuth—and sulfur-codoped TiO_2 ," *Journal of Physical Chemistry C*, vol. 112, no. 17, pp. 6620–6626, 2008.

[41] W. E. Morgan, W. J. Stec, and J. R. Van Wazer, "Inner-orbital binding-energy shifts of antimony and bismuth compounds," *Inorganic Chemistry*, vol. 12, no. 4, pp. 953–955, 1973.

[42] J. Wang, L. Jing, L. Xue, Y. Qu, and H. Fu, "Enhanced activity of bismuth-compounded TiO_2 nanoparticles for photocatalytically degrading rhodamine B solution," *Journal of Hazardous Materials*, vol. 160, no. 1, pp. 208–212, 2008.

[43] J. Huang, X. Wang, Y. Hou et al., "Synthesis of functionalized mesoporous TiO_2 molecular sieves and their application in photocatalysis," *Microporous and Mesoporous Materials*, vol. 110, no. 2-3, pp. 543–552, 2008.